33RD CONGRESS
OF THE INTERNATIONAL COUNCIL
OF THE AERONAUTICAL SCIENCES
STOCKHOLM, SWEDEN, 4-9 SEPTEMBER, 2022

ICAS 2022 SWEDEN

EXPLORATION OF BOX-WING AIRCRAFT CONCEPT USING HIGH-FIDELITY AERODYNAMIC SHAPE OPTIMIZATION

Pedro D. Bravo-Mosquera[1,2], Timothy Chau[2], Fernando M. Catalano[1] & David W. Zingg[2]

[1]São Carlos School of Engineering - University of São Paulo (EESC-USP), São Carlos, SP, Brazil, 13563-120
[2]Institute for Aerospace Studies - University of Toronto, Toronto, Ontario, Canada, M3H 5T6

Abstract

This paper presents an exploration of the aerodynamic design of a box-wing aircraft concept through high-fidelity aerodynamic shape optimization. The optimization framework consists of B-spline parameterization surfaces, an integrated mesh parameterization and deformation scheme based on the theory of linear elasticity, free-form and axial deformation geometry control, a Newton-Krylov-Schur flow solver for the Reynolds-averaged Navier-Stokes equations, a gradient-based optimizer, and the discrete-adjoint method for gradient evaluation. These modules are integrated in an aerodynamic shape optimization framework called Jetstream, which is used to minimize the cruise drag of a single-aisle, medium range box-wing aircraft at transonic flight conditions (Mach = 0.78) with lift, trim, and minimum wing volume constraints. The drag of the optimized box-wing configuration is about 10% lower than the initial concept due to reduced wave drag from the near elimination of shocks and reduced induced drag from an optimal spanwise lift distribution. These results demonstrate the potential aerodynamic advantages of the box-wing concept, and the importance of high-fidelity analysis and optimization tools towards the development and evaluation of novel configurations that can lead to reduced fuel burn and emissions.

Keywords: Box-Wing; Induced drag; Aerodynamic shape optimization; Discrete-adjoint method; Multidisciplinary design optimization

1. Introduction

According to the International Air Transport Association (IATA), aviation is the second fastest growing source of emissions of all modes of transport. Those emissions contribute to changing the energy balance of the atmosphere, which can be harmful to human health in a medium-term period. Although at this time airlines only represent 2-4% of climate change causing emissions, if aviation continues on its current growth path, this share will increase to more than 20% in 2050 [1]. Several design strategies have been proposed to reduce aviation's environmental impact by implementing technologies that reduce fuel consumption. From a design perspective, lighter manufacturing materials and high bypass ratio engines have demonstrated reductions in fuel burn of new conventional aircraft. Disruptive technologies such as unconventional aircraft configurations, hybrid-electric propulsion systems, and alternative fuels are also objectives of current investigations [2]. In contrast, other strategies to ensure effective fuel usage include adequate aircraft maintenance and increased airspace efficiency by reducing the number of flights to and from each airport. In this context, the industry's long-term decarbonization goal is being aided by novel aircraft design, new engine technology, and improved air traffic management.

Many airlines are well aware of these issues and are making significant investments in carbon reduction efforts. According to an examination of airline records, the fuel-burn of current conventional aircraft is usually four liters per passenger per 100 km, representing around 30% of Direct Operating Cost (DOC) [3]. Therefore, the relationship between fuel-burn and aircraft capability, in terms of

design speed, payload capacity (mass and/or volume), and range, concerns directly to the aircraft manufacturer, since the appropriate trade-off among those variables determines the entire performance of the aircraft. For example, if the design speed or range is increased, the fuel consumed per passenger-km tends to increase. In contrast, the fuel burn per passenger-km decreases for aircraft capable of transporting a larger number of passengers. For this reason, novel aircraft configurations that allow for the transportation of the greatest number of passengers with the least amount of fuel provide financial advantages for airlines to buy greener aircraft.

One of the most relevant unconventional configurations dealing with this aspect is the Blended Wing Body (BWB). According to Liebeck [4], an 800-passenger BWB can offer a remarkable reduction in fuel-burn per passenger-km of about 27% compared to a conventional baseline configuration over a 13000 km range. A subsequent study focused on a 450-passenger capacity design, which showed 32% lower fuel-burn per seat-mile when compared to the Airbus A380. The Box-Wing (BW) concept, which is the focus of this paper, also offers the possibility to increase the number of passengers thanks to its low wing loading, allowing to increase the fuselage dimensions for more payload-carrying structure. A current example of this approach is the PrandtlPlane aircraft, a BW concept designed for short-to-medium range missions, which allows the number of passengers to be increased from below 200 (similar to a narrow-body aircraft) to more than 300 (similar to a wide-body aircraft) within the gate C constraint [5]. In this particular case, by increasing the number of passengers by about 66%, it is possible to obtain a reduction of fuel per passenger up to 22%, representing a global warming potential reduction of about 17% [6, 7]. Such results have been obtained from several design and optimization strategies, using mainly low and medium fidelity tools by means of multidisciplinary approaches [8]. Carini et al. [9] presented the only attempt at using high-fidelity optimization tools in a thorough iterative design of the PrandtlPlane aircraft. In this case, the authors implemented an Euler-equation-based optimization study to minimize drag with respect to both twist and camber design variables.

Since the introduction of Prandtl's "best wing system" in 1924 [10], the particular characteristics of the BW concept, i.e., its potential for induced drag reduction has motivated researchers to investigate its aerodynamic performance using different levels of physical fidelity. For example, Kroo [11] investigated the aerodynamic efficiencies of several nonplanar wings of fixed span and vertical tip extents using low-fidelity aerodynamics. He found that the BW layout outperformed all others, reaching a span efficiency factor (e) on the order 1.46. Demasi et al. [12] studied in detail the induced drag theorem of box-wings using a vortex panel method. The authors proved that an optimal distribution of total lift on the fore, aft, and vertical wings reduces induced drag by 40% compared to conventional cantilever wings. Russo, Tognaccini, and Demasi [13] provided details of the aerodynamic drag breakdown of a BW in subsonic and transonic regimes using numerical flow solutions obtained by Reynolds-averaged Navier-Stokes (RANS) analyses. The main contribution of this work is that the induced drag of box-wings simulated in viscous and compressible flows is equivalent to that anticipated by inviscid and linear aerodynamic theories. In this case, for a fixed lift coefficient, the viscous drag of a box-wing is 26% higher than the one of the elliptical wing, whereas a benefit of 46% in terms of induced drag is obtained.

This result is in line with previous aerodynamic shape optimization studies of box-wings, in which Euler-based [14, 15] and RANS-based [16] approaches have been implemented to minimize drag considering prescribed design variables and constraints. In both cases, the box-wings were able to redistribute the total lift from one wing to the other, satisfying several design constraints, while simultaneously improving aerodynamic performance. It is worth mentioning that the optimizer designed supercritical cambered airfoils with very weak shocks, while introducing an optimal twist distribution that minimized induced drag. Though these studies offered insights into the performance of BW configurations, they were limited by only considering the closed-wing surface itself, i.e., these efforts did not account for wing-fuselage interaction to capture interference drag effects, such as separation around the junction, as well as trim effects.

The objective of the present study is therefore to further understand the aerodynamic design and performance potential of a BW configuration, including the fuselage geometry, in order to account for wing-body flow interactions and proper fuselage lift through aerodynamic shape optimization based on the RANS equations. In particular, drag minimization is applied to the aerodynamic design and performance evaluation of a BW aircraft based on the Airbus A320neo. The RANS-based aerodynamic shape optimization provides an accurate quantification of the trade-offs between induced drag and viscous drag for the BW aircraft concept, thus complementing previous low-fidelity conceptual design and optimization efforts [5, 6, 17, 18, 19, 20, 21, 22].

The paper is organized as follows. Section 2 provides a brief overview of the methodologies implemented to design and evaluate the proposed BW concept, including details of low-fidelity conceptual-level Multidisciplinary Design Optimization (MDO) frameworks that were used to evaluate different design alternatives at an early phase of the design process, as well as details of the high-fidelity aerodynamic shape optimization framework based on the RANS equations. Section 3 describes the problem setup for the aerodynamic shape optimization problem and includes details on aircraft size, initial geometry, computational mesh, and geometry control. Section 4 presents the results for the exploration of the lift-constrained drag minimization of the BW concept, as well as details of the performance analysis based on aircraft mission profile. Conclusions and suggestions for future work are given in Section 5 and Section 6, respectively.

2. Methodology

In this section, the computational tools that were used to design and assess the single-aisle medium-range BW aircraft are presented. The section is organised into subsections that describe how these tools were employed towards the development of a BW concept with reduced drag.

2.1 Conceptual-level Multidisciplinary Design Optimization

Conceptual design is an early phase of the design process and includes both design space exploration and evaluation of different design alternatives. This phase requires tools that are fast but accurate enough to evaluate different design alternatives and provide some initial estimations of system performance. In this section, we briefly introduce two conceptual design frameworks that were used to design and evaluate the BW concept.

2.1.1 Paerom

Paerom was used to define the main characteristics of the aircraft, such as its wingspan (32.2 m), height-to-span ratio (0.244), stagger-to-span ratio (0.7), among others. This tool is a low-fidelity conceptual design Multidisciplinary Design Optimization (MDO) framework that assists in the initialization of an aircraft based on top-level requirements and user-defined parameters such as propulsion system type, configuration, and specific airframe elements. Paerom features several analysis modules that help to estimate aircraft aerodynamics, weights, stability, and mission performance [23, 24].

After the initial sizing and sensitivity analyses, a single-objective optimization of the BW concept was performed to investigate the relationship between fuel burn per passenger-km as a function of aircraft size. The nominal range is 1852 km plus 805 km for reserve and the maximum number of passengers is set equal to 165. The Matlab Genetic Algorithm (GA) was used to perform the aircraft optimization. Design variables included wing geometric properties such as aspect ratio, height-to-span ratio, stagger-to-span ratio, among others, as well as performance characteristics such as initial cruise altitude, wing area, and maximum required thrust, while design constraints were set based on top-level requirements and operational characteristics such as the available wing fuel volume. The final configuration of the BW concept that corresponds to the selected design point is shown in Fig. 1. Table 1 provides a summary of the aircraft characteristics, while additional details are presented in [24].

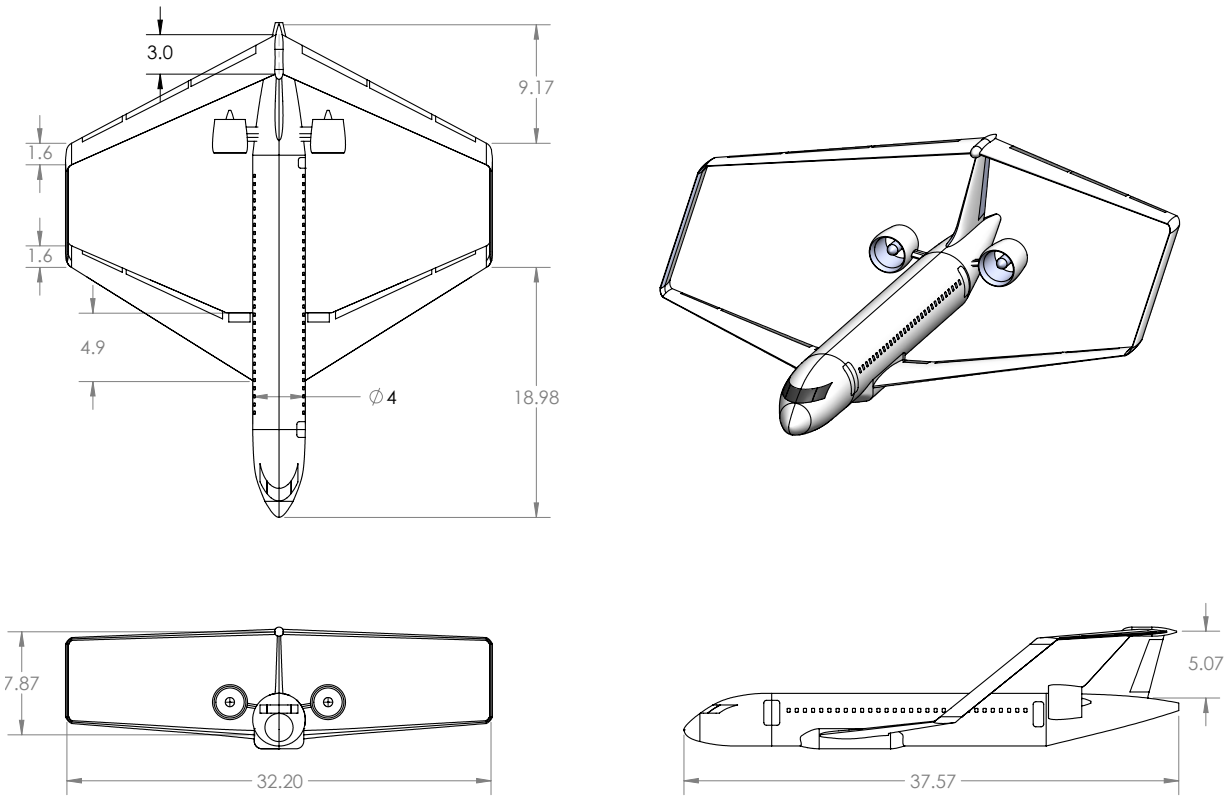

Figure 1 – Views of the box-wing configuration (version with podded engines), with dimensions in meters.

Table 1 – Box-wing aircraft characteristics.

Requirements and features	Notes
Passengers = 165	Value refers to a typical single-aisle medium-range aircraft.
Nominal range [km] = 1852 + 805	Maximum nominal range plus diversion range at specified payload.
Cruise Mach [-] = 0.78	Minimum value of cruise Mach.
Initial cruise altitude [m] = 12500	Initial cruise altitude after design optimization.
Maximum take-off mass [kg] = 78978.8	Value obtained using fuel-burn as objective function.
Empty mass [kg] = 44982.1	Obtained by means of low-fidelity weight estimation methods.
Cruise L/D [-] = 19.3	Obtained by means of low-fidelity aerodynamics.
Fuel mass [kg] = 7886.7	For nominal range.

2.1.2 Faber

Faber is a mixed low- and medium-fidelity MDO tool that provides a means for the systems analysis, sizing, and optimization of transport aircraft, with a focus on developing aircraft that are representative of a given configuration and class [25]. Aircraft configurations include the conventional tube-and-wing (CTW), as well as more unconventional aircraft configurations such as the BW. Given an initial concept and a set of design missions and top-level aircraft requirements, physics-based methods are used to iteratively size and analyze the aircraft components and subsystems. This iterative routine is further incorporated into a gradient-based optimization framework to refine the initial concept for minimum fuel burn.

In this work, Faber is primarily used to recompute the structural wing mass of the BW concept using its equivalent beam model. These results are then used to improve the weight estimate from Paerom, which uses a regression analysis based on finite element analysis data obtained from an idealized box wing structure [26]. Faber also includes a global buckling detection method based on Euler-Bernoulli beam theory, currently not available in Paerom, which aids in sizing box wing structures subjected to compressive axial loads.

For this study, the objective is to minimize the block fuel consumption of the aircraft. In order to maintain the wing planforms obtained from Paerom, design variables only include thickness-to-chord ratio and chord degrees of freedom at major stations across the wing. Constraints include minimum wing volume, which ensures that there is enough space in the wing system to contain the fuel tanks, minimum tip chord lengths, which prevent the optimizer from creating a wing with unrealistic wing taper ratios, and buckling constraints, which ensure that each wing segment does not fail due to buckling. For structural sizing and analysis, the vertical wing segment is modeled as a series of bar elements, while rigid joints are used to define its connections with the fore and aft wings. Figure 2 shows details of the BW concept simulated in Faber.

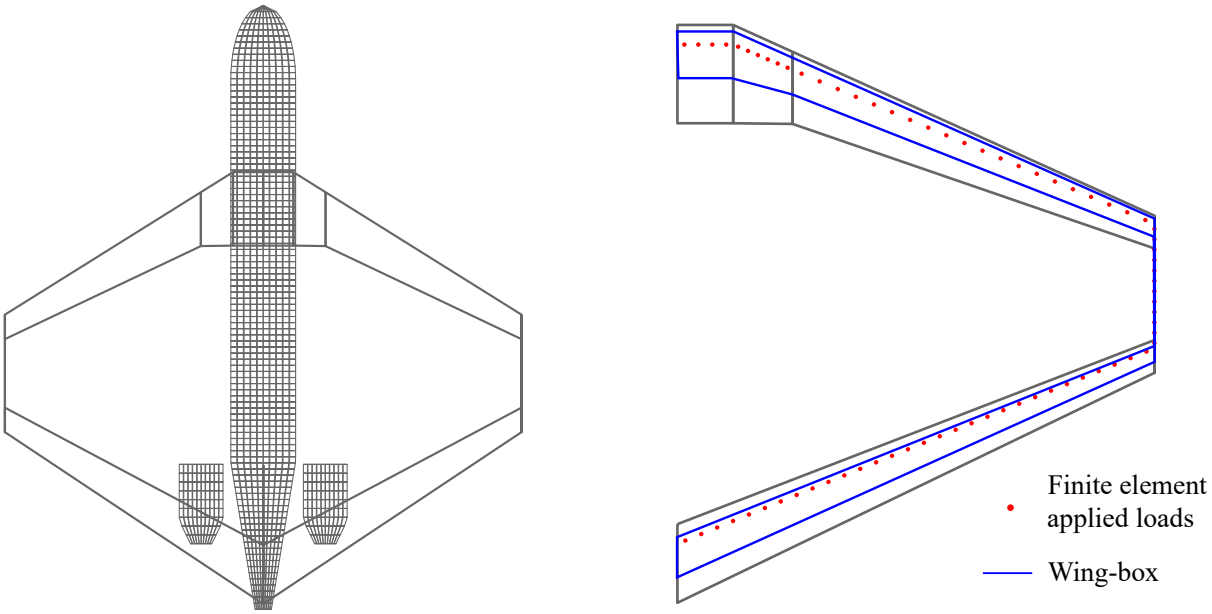

(a) Conceptual design - BW planform.

(b) Beam element discretization and wing-box sizing.

Figure 2 – Overview of the BW concept simulated in Faber.

2.2 High-Fidelity Aerodynamic Shape Optimization Framework - Jetstream

The high-fidelity aerodynamic shape optimization framework used in this study is called Jetstream. The methodology involves four main components: an integrated mesh parameterization and deformation scheme [27], a free-form and axial deformation geometry control system [28], a structured multiblock parallel implicit Newton-Krylov-Schur flow solver for the RANS equations fully coupled with the Spalart-Allmaras turbulence model [29], and the discrete-adjoint method for gradient evaluation [30, 31], and SNOPT for gradient-based optimization [32]. This framework has been used to explore several unconventional configurations, combining considerable geometric flexibility with frequently unknown design spaces in the pursuit of a viable solution for aviation sustainability. Some key examples include: Strut-Braced Wing (SBW) concepts [25] and Hybrid Wing–Body (HWB) geometries [33, 34]. A brief overview of each component is provided in this section.

2.2.1 Geometry Parameterization, Control, and Mesh Movement

For geometry control and mesh deformation, a two-level system is used, which consists of a free-form and axial deformation geometry control system [28], and an integrated mesh parameterization and deformation method [27]. Starting with an initial structured multiblock mesh, each block is parameterized with cubic B-spline volumes whose B-spline control points can be manipulated to deform the parameterized grid. This is achieved through a robust linear-elasticity model applied to the coarser grid of B-spline control points that can then be used to regenerate the deformed CFD grid algebraically.

Although the B-spline control points defining the aerodynamic surfaces can be manipulated directly, the number of degrees of freedom are reduced to fewer and more practical design variables by embedding these B-spline control points within free-form deformation (FFD) volumes. These FFD volumes are themselves B-spline volumes whose control points can be moved to deform the embedded shape in a continuous manner. This is achieved through rotation and translation operators applied to the FFD volume control points, which provide twist, taper, and cross-sectional shape design variables. Attached to each FFD volume is an axial curve, defined as a B-spline curve of any order and normally located at either the leading edge, trailing edge, or quarter-chord of a wing geometry. These define the local coordinate systems that are referenced by the FFD volume design variables, and can be used to drive the overall shape and orientation of the FFD volumes through span, sweep, and dihedral degrees of freedom if desired. The control points of the FFD volumes and axial curves are the used to control the location of the B-spline control points of the geometry parameterization, enabling an analytical geometry representation throughout the optimization process.

2.2.2 Flow Solver

Jetstream uses a parallel, implicit, multi-block structured finite-difference solver called Diablo. This flow solver is capable of solving either Euler [35] or RANS [29] equations. Second-order summation-by-parts (SBP) operators with scalar or matrix numerical dissipation are used to discretize the equations, while boundary conditions and block interfaces are enforced using simultaneous approximate terms (SATs). The combination of SBP and SATs operators provides excellent numerical stability properties and efficient parallel performance [36]. For RANS analyses, the equations are closed with the Spalart-Allmaras one-equation turbulence model [37].

The flow solver is based on a parallel Newton-Krylov-Schur algorithm that generates the initial iteration for the subsequent inexact-Newton phase using an approximation Newton start-up phase. As a result, the system of linear equations generated in both phases is solved using a flexible generalized minimal residual algorithm (GMRES) with an approximate-Schur parallel preconditioner. Additional details of the solver can be found in Osusky et al. [29]. Note that Diablo has been validated using the NASA Common Research Model wing-body configuration from the fifth Drag Prediction Workshop [38].

2.2.3 Optimization Algorithm and Gradient Evaluation

Numerical problems involving aerodynamic shape optimization, particularly in three dimensions, are typically associated with a large number of design variables [39]. For optimization, etstream uses the discrete adjoint method for computing objective function and constraint gradients that depend on the flow solution. The advantage of this approach is that the cost is almost independent of the number of design variables [30, 31]. Jetstream uses SNOPT (Sparse Nonlinear OPTimizer) [32], a gradient-based optimizer that uses the sequential quadratic programming method. For gradient evaluation, the discrete-adjoint method is used for gradients that depend on the flow solution or mesh deformation scheme. For all other sensitivities, gradients are calculated analytically or approximated through the complex step method.

3. High-Fidelity Aerodynamic Shape Optimization Problem

In this work, the optimization objective is to minimize drag for the BW concept described above. An exploratory optimization is performed to investigate aerodynamic trends and trade-offs, and to refine the initial geometry using aerodynamic shape optimization. The problem is formulated for a given Mach number, lift coefficient, and wing planform. In this context, the focus in on modifications in airfoil shapes and spanwise twist distributions, whereas the taper, sweep, span, and dihedral of the closed-wing remain constant. This strategy is applied over the whole closed-wing system, including the blended transitions that join the fore and aft wings with the vertical wing.

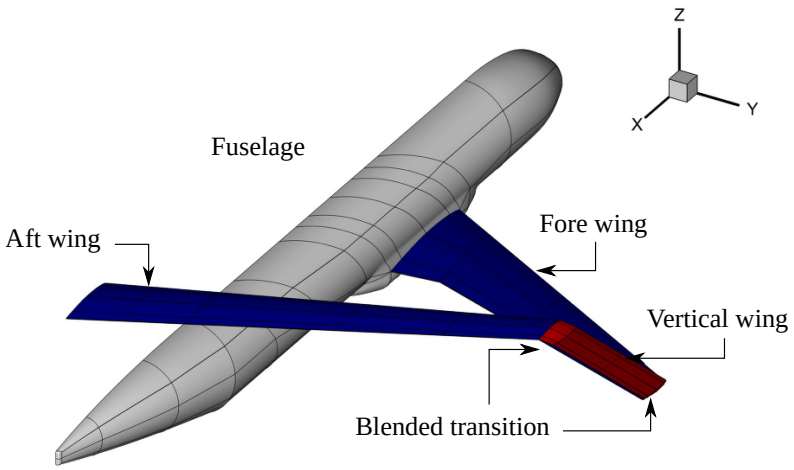

Figure 3 – Baseline BW configuration for high-fidelity aerodynamic shape optimization.

Table 2 – Geometric characteristics used for high-fidelity optimizations[1].

Parameter	Fore wing	Aft wing	Vertical wing
Planform area[2,3] $[m^2]$	51.8	36.5	9.3
Span $[m]$	16.1	16.1	5.7
Mean aerodynamic chord $[m]$	3.19	2.39	1.6
Aspect Ratio [-]	5.0	7.1	3.5
Taper Ratio [-]	0.31	0.54	1.0
Dihedral angle $[deg]$	4°	-2°	90°
Leading edge sweep angle $[deg]$	32°	-28°	50°

[1] Half-model dimensions.
[2] Portion inside the fuselage included for fore wing.
[3] Not including blended transitions.

3.1 The Baseline BW Concept

The geometry consists of two main components: fuselage and box-wing. The fuselage geometry is kept unchanged in this work, whereas the complete box-wing is optimized along with the patches of the fairing where the fore wing is attached. The length of the fuselage and its diameter are 37.57 m and 4.0 m, respectively. Patch topologies of the BW concept are illustrated in Fig. 3, and the main dimensions of each box-wing component are summarized in Table 2.

3.2 Computational Grid

The computational domain is discretized using a structured multiblock grid (O-O blocking topology), which is then fitted with B-spline volumes for mesh deformation. The baseline structured multiblock grid is created with ICEM-CFD [40] and consists of 970 blocks with 21.18 million nodes. The first step was to divide the physical region into sub-regions, each bounded by six faces in 3D. This step requires considerable user interaction in order to get a successful domain decomposition (e.g., with block edges aligned with complex geometric surfaces).

Figure 4 shows the structured surface mesh of the BW configuration. The orthogonality metric has values larger than 0.6, indicating a good mesh orthogonality near the solid surfaces [40]. This mesh is suitable for optimization, as it produces good convergence to steady state, provides a good balance between accuracy and time to convergence, and leads to high-quality meshes even when deformed during optimization.

In order to obtain performance estimates with reduced numerical error, a grid refinement study based on Richardson extrapolation is completed for the optimized geometry, using grids with roughly 40 (L1) and 80 (L2) million nodes in addition to the optimization grid (L0). The grids were created using Jetstream's automatic grid refinement capabilities, which use grid node insertion and redistribution to

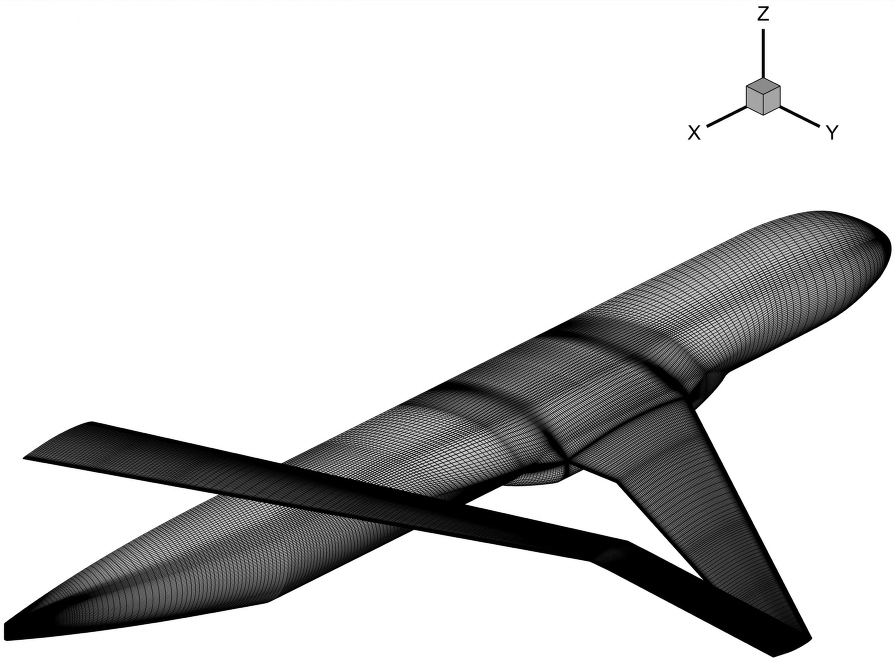

Figure 4 – Structured surface meshes of the primary components of the aircraft.

Table 3 – BW grid information[1].

Refinement level	Number of nodes	Average Off-wall spacing[2]	Average y+
L0	21.18×10^6	1.17×10^{-6}	0.59
L1	40.73×10^6	8.79×10^{-7}	0.45
L2	81.46×10^6	6.79×10^{-7}	0.34

[1] Calculated for Reynolds number equal to 14.23×10^6.
[2] Off-wall spacings are in units of mean aerodynamic chord.

keep the original mesh spacing functions while maintaining the analytical surface definition [29]. Table 3 lists some properties of the three meshes. All performance results presented below are estimated grid-converged values obtained via Richardson extrapolation.

3.3 Geometry Parameterization and Control

For geometry control, the free-form and axial deformation method [28] is used, where the B-spline control points are embedded within free-form deformation (FFD) volumes that provide twist and section shape design variables. The free-form and axial deformation geometry control system is shown in Fig. 5. The blue spheres are FFD control points, and the green spheres are axial control points. The aerodynamic surfaces are embedded within 6 FFD volumes: two for the fore wing, one for the aft wing, one for the vertical tip fin, and one for each blended transition. A patch-based junction deformation scheme [29] is also included to allow deformations over the fore wing to propagate to adjacent fuselage patches, which are left unembedded. The FFD volumes of the fore wing, aft wing, and vertical tip fin each consist of 11, 10, and 10 FFD-volume cross-sections, respectively, while those of the blended transitions each include 5 FFD-volume cross-sections. This yields a total of 38 unique FFD-volume cross-sections, even accounting for overlaps. Each FFD-volume cross-section has 20 equally spaced FFD control points, 10 on each side of the aerodynamic surfaces. Linear axial curves are positioned at the quarter chord of the fore and aft wings and the vertical tip fin, whereas cubic axial curves are attached to the quarter chord of the two blended transitions, resulting in 11 axial curve control points. In this work, these axial curves are primarily used to define the points of rotation for the twist design variables.

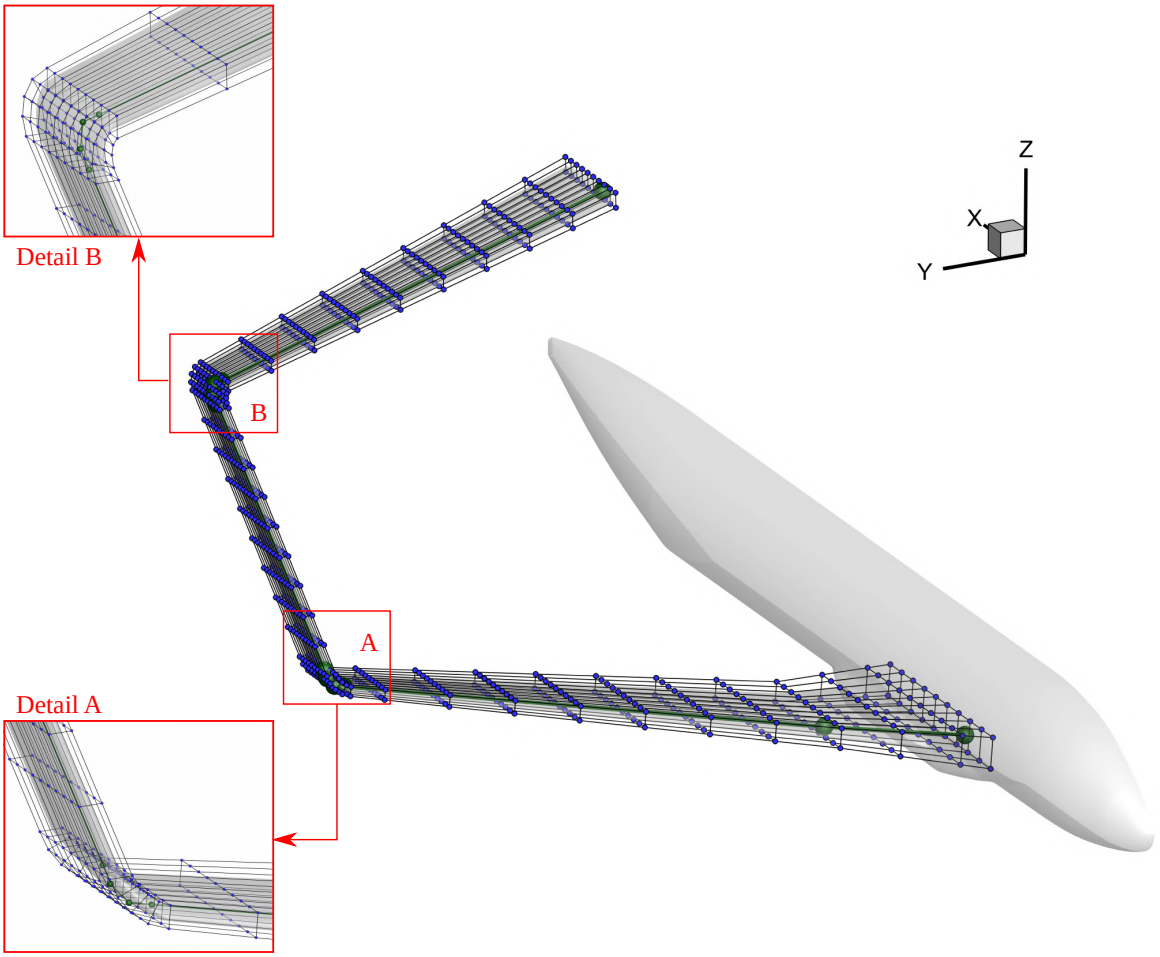

Figure 5 – Geometry control systems with FFD volume entities.

3.4 Optimization Problem Formulation

The goal of this study is to minimize the drag coefficient for a certain flight condition, i.e., $C_L = 0.51$, Mach number of 0.78, altitude of 12500 m, which corresponds to a Reynolds number of 16.57×10^6, based on a MAC of 2.55 m. The optimization problem can be stated as:

$$\begin{aligned} \text{min} \quad & \mathscr{J}(\mathbf{v},\mathbf{q},\mathbf{b}^{(m)}) \\ \text{with respect to} \quad & \mathbf{v} \\ \text{subject to} \quad & \begin{cases} \mathscr{M}^{(i)}(\mathbf{v},\mathbf{b}^{(i)},\mathbf{b}^{(i-1)}) = 0, \quad i = 1,2,...,m \\ \mathscr{R}(\mathbf{v},\mathbf{q},\mathbf{b}^{(m)}) = 0 \\ \mathscr{C}_e(\mathbf{v},\mathbf{q},\mathbf{b}^{(m)}) = 0 \\ \mathscr{C}_i(\mathbf{v},\mathbf{q},\mathbf{b}^{(m)}) \geq 0 \end{cases} \end{aligned} \tag{1}$$

where $\mathscr{J}$ is the objective function, computed by $C_D S$, where S is the nondimensional planform area of the box-wing, which cannot be changed during optimization, $\mathbf{v}$ are the design variables, $\mathbf{q}$ are the flow variables, $\mathbf{b}^{(m)}$ are the control points of the B-spline volume in which the grid is embedded, $\{\mathscr{M}^{(i)}\}_{i=1}^{m}$ are the mesh movement equations, which are solved for $\mathbf{b}^{(i)}$, i.e. the B-spline volume control points at the ith increment, $\mathscr{R}$ is the flow residual, and $\mathscr{C}_e$ and $\mathscr{C}_i$ are additional equality and inequality constraints, respectively, which can be either linear or nonlinear. A summary of the design variables and their bounds, as well as a list of the linear and nonlinear constraints is presented in Table 4.

The objective of the optimization is to minimize drag subject to lift and pitching moment constraints, in addition to some geometric constraints described below. Lift is constrained to be equal to the weight

at the start of cruise, and the pitching moment about the center of gravity must be zero. The wing volume is constrained to ensure that sufficient fuel can be stored in the fore and aft wings. Thickness constraints are active at several locations along the chord and are relative to the initial value. Finally, a linear twist interpolation over each blended transition is imposed in order to prevent the optimizer from designing blended transitions with large curvature, avoiding interference effects with the main wings. Such an approach makes for flexible design spaces that are well-suited for exploratory shape optimization.

4. Results

4.1 Optimization convergence history

For tracking convergence, SNOPT provides a number of metrics: feasibility, optimality, and the merit function. The merit function is the objective when constraints are satisfied, whereas feasibility and optimality represent the constraint satisfaction and the gradient of the augmented objective function, respectively. The optimization convergence history for the BW optimization is shown in Fig. 6. After 187 iterations, the merit function is sufficiently converged to achieve engineering precision, feasibility has been reduced to below 10^{-6}, and optimality has been reduced by at least two orders of magnitude.

Table 4 – Design variables and constraints for high-fidelity aerodynamic shape optimization.

Optimization Problem	Function / Variable	Description	Lower Bound	Upper Bound
Minimize	C_D	Drag coefficient		
with respect to	Angle of attack (α)	The angle of attack is limited to $\pm\,3^\circ$, based on deck angle requirements.	-3°	3°
	Twist (τ)	Twist of each FFD section.	-10°	10°
	Section Shape (Δ_z)	Vertical displacements of the FFD control points for airfoil-shape control.	0.5	2.0
Design variables	**799**			
	Constraint	Description		Value
subject to	Lift	Lift constraint at the start of cruise (nonlinear).		$C_L = 0.51$
	Trim	Aircraft pitching moment constraint equal to zero (nonlinear).		$C_M = 0$
	Wing volume	Minimum box-wing OML volume constraint based on fuel storage requirements (nonlinear).		$Vol = Vol_t$
	Wing thickness	Minimum thickness constraints between each pair of FFD-volume control points (linear).		$t/t_0 \geq 0.5$
	Linear twist	Links the twist design variables of the blended transition segments (linear).		-
Constraints	**1117**			

4.2 RANS-Based Aerodynamic Shape Optimization

This section describes the comparisons of aerodynamic characteristics between the baseline and optimized configurations under the cruise condition. For the baseline geometry, the selected airfoils are the NASA SC(2)-0412 (fore wing root), -0410 (fore wing crank and tip), -0410 (aft wing root to tip), and -0010 (vertical tip fin). These airfoils are characterized by a large leading-edge radius, and a reduced curvature over the middle region of the upper surface, which helps to delay the shock. The wing segments are initially untwisted and those intersecting the fuselage have angle of incidence equal to 1°. This provides a starting geometry for optimization and valid conceptual level estimates of various quantities. Fig. 7a shows the front views of the baseline and optimized geometries with shock surfaces highlighted in red. The shock surfaces over the upper surface of the fore wing have been mostly removed. A strong shock wave appearing close to the root of the baseline aft wing has also been largely eliminated following optimization. Likewise, Fig. 7b illustrates the surface pressure

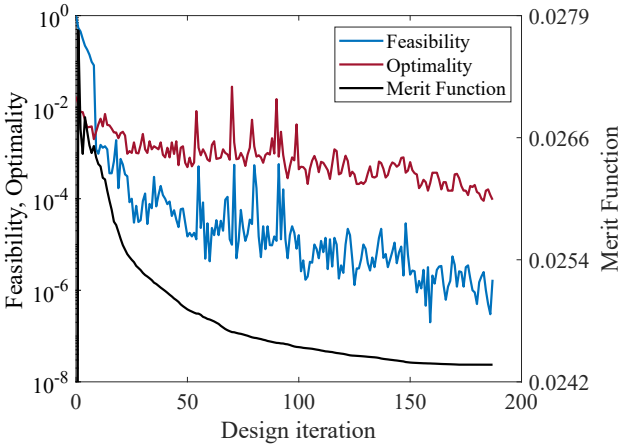

Figure 6 – BW concept: Optimization history. The merit function represents C_D.

coefficient contours of the baseline and optimized configurations of the box-wing with L0 grid, clearly showing that the C_p lines are distributed more evenly in the optimized geometry. The baseline concept has an angle of attack of 3° at the initial cruise flight condition, where C_L = 0.51, and C_D = 0.0269. The optimized concept reached an angle of attack of 3°, C_L = 0.51, and C_D = 0.0244, meaning that the optimizer tends toward flying at the maximum angle of attack permitted. The reduction in the drag coefficient is over 10%.

The corresponding pressure coefficient distributions and section shapes of the fore wing and aft wing at various spanwise locations are given in Fig. 8 and Fig. 9, respectively. For the baseline fore wing geometry, the sudden increase in pressure coefficient at about 50–60% of chord is due to the shock. However, the optimized section shapes greatly reduced shocks, demonstrating a reduction in wave drag. In these results, the original volume is redistributed by thickening the wing sections near the root, which is typical for aerodynamic shape optimization problems where the minimum volume is a design constraint [25]. On the other hand, the baseline aft wing has weaker shocks than the fore wing. This is because the aft wing is more lightly loaded, i.e. has a lower C_L. In this case, it can be seen that the optimizer has designed supercritical cambered airfoils with smoother pressure recoveries, especially along the trailing edge.

As far as the minimization of induced drag is concerned, acting on the twist distribution allows to modify the spanwise lift distribution to get it closer to the one of optimal solutions [41]. In this case, the fore and aft wings are characterized by wash-out (i.e., decreasing the incidence angle from the wing root out to the wing tip) and wash-in (i.e., increasing the incidence angle from the root to the tip), respectively. The optimized results are consistent with those of past studies and with theoretical results, providing a reliable estimate of the performance of the BW aircraft [14, 16].

Figures 10 and 11 illustrate the surface pressure contours and pressure distributions, respectively, across the vertical wing. The baseline geometry presents an adverse pressure gradient in the intersection with the blended transition of the fore wing ($x/h = 0\%$). However, the optimizer designed supercritical airfoils with a more favorable pressure gradient. The other sections of the vertical wing did not present a significant difference in the pressure distribution, despite their modification on the twist distribution that changed gradually from inboard to outboard from the bottom to the top of the vertical tip fin. This results in a wing design that is similar to those that can be found in the literature [6, 18], in which the side-force distribution over the vertical wing forms the signature closed-loop circulation pattern, as shown in Fig. 12. This result is also consistent with the incompressible Prandtl formula for the lift-induced drag of an elliptical wing, which has demonstrated

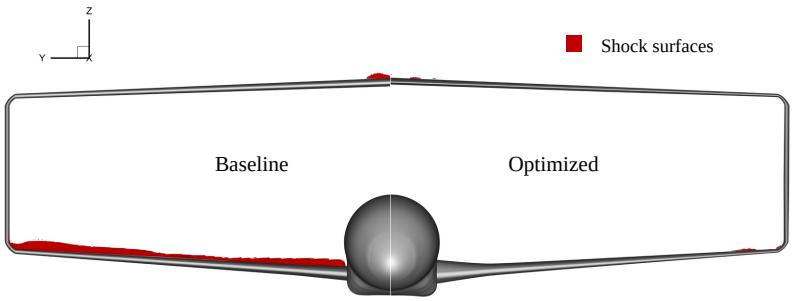

(a) Shock surfaces for the baseline (left) and optimized (right) box-wing configuration.

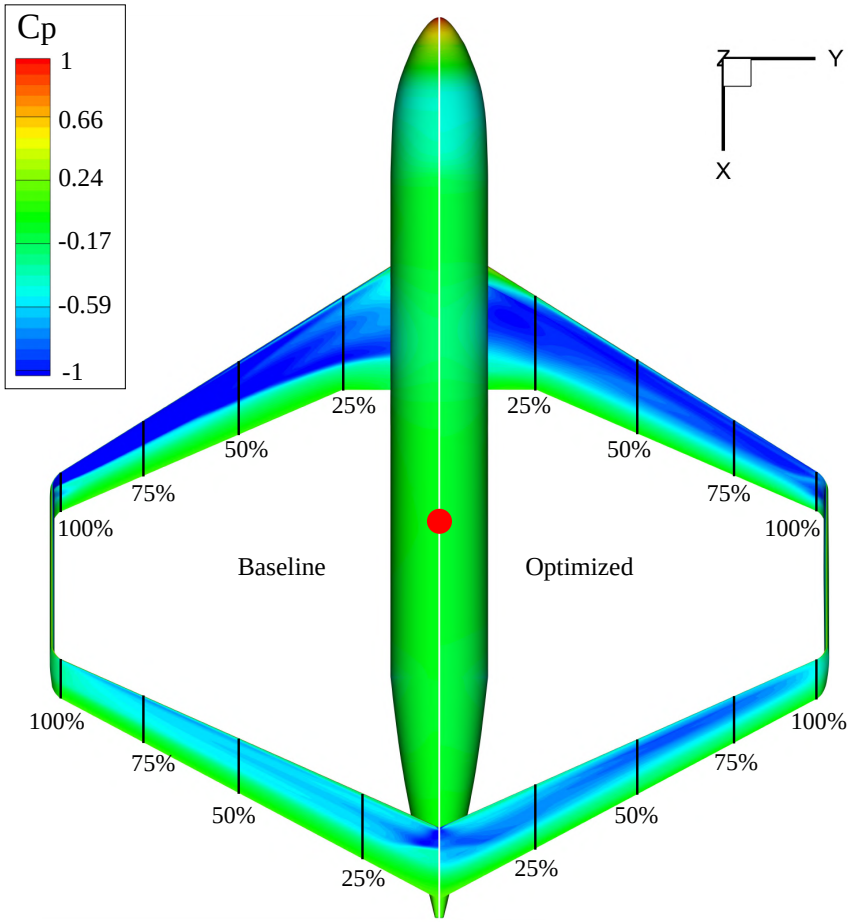

(b) Surface pressure coefficient contours for the baseline (left) and optimized (right) box-wing geometries (Top views of fore and aft wings. The red sphere represents the CG).

Figure 7 – Box-Wing configuration: Optimization results: $\alpha = 3.0°$, $C_L = 0.51$, $C_D = 0.0244$, $L/D = 20.9$.

very good agreement with the vortex-force-based definition of lift-induced drag, even in presence of shocks [10, 11, 13]. This approach was used in the very initial stage of the aircraft design, which means that there is a solution of minimum induced drag for a fixed lift and height-to-span ratio before applying high-fidelity aerodynamic shape optimization.

Given that fully turbulent flow has been assumed and the box-wing area is highly constrained, the optimizer is not able to reduce the friction drag in this case, so the drag reduction on the BW concept is due to wave and induced drag reductions. Also visible in Fig. 12, the current optimization demonstrated the unique capability of the BW concept to redistribute its optimal lift distribution whereas trim and other constraints are satisfied. As a result, the condition of minimum induced drag of the box-wing configuration is valid even though the lift on the fore and aft wings is different, and the lift

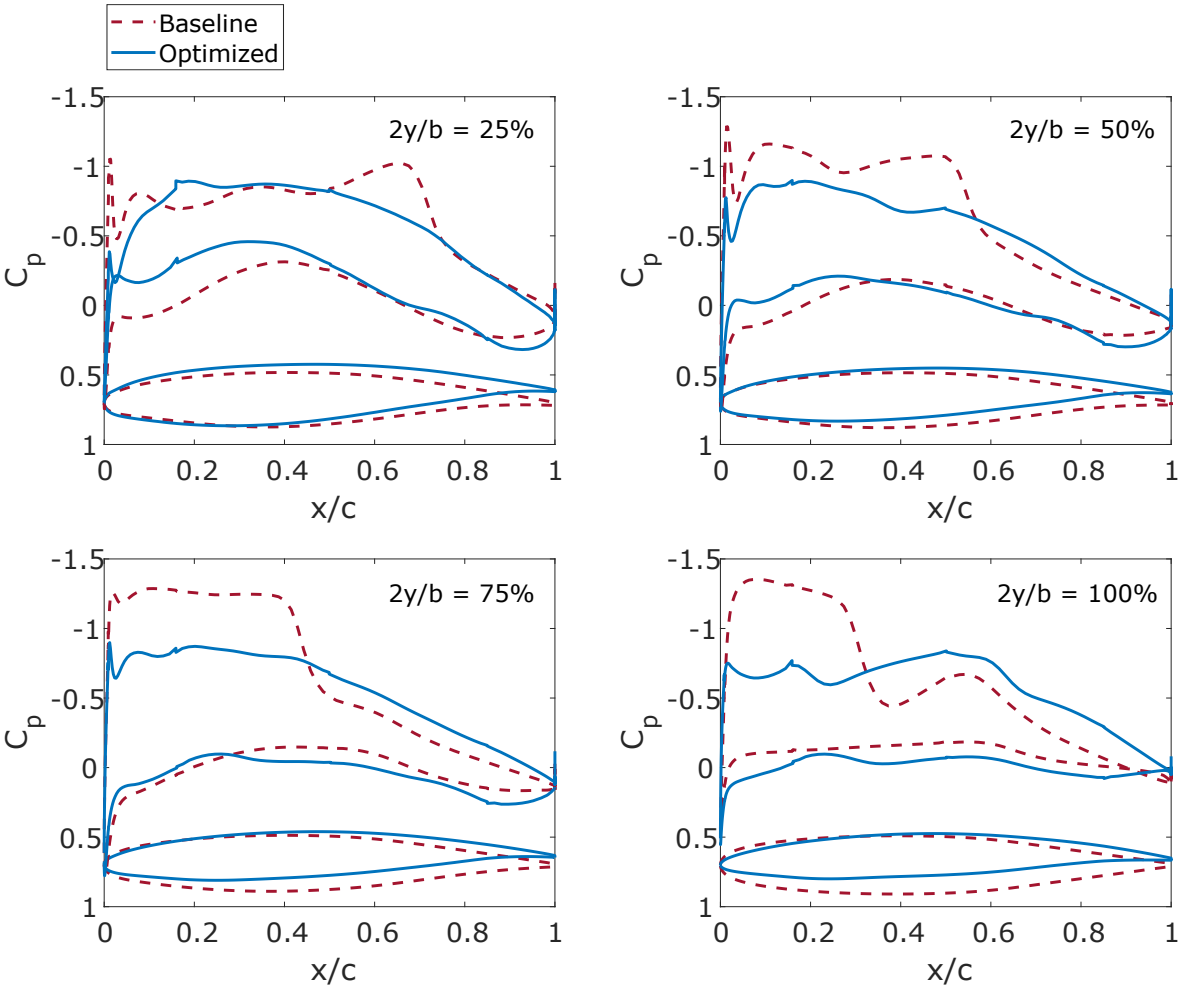

Figure 8 – Pressure distributions on the baseline and optimized box-wing designs (fore wing).

across the vertical wings is distributed proportionally.

Plane cuts of the normalized z-component of momentum are plotted one MAC length downstream of the baseline (Fig. 13a) and optimized (Fig. 13b) wing geometries. The figures clearly show that the optimized geometry reduced the strength and magnitude of the tip vortex. This result suggests that induced drag is minimized due to the smaller induced velocities.

4.3 Weight estimation and performance studies

The structural weight estimation (wing metallic structures) has been assessed by means of the FEM-based procedures described in Section 2.1.2 The non-structural components and fuselage weights have been assessed through statistical methods, as described in [42], whereas the payload weight has been evaluated considering the maximum number of passengers (165 pax) and a standard weight of 100 kg assigned to each passenger. The main mass breakdown for the BW configuration is reported in Table 5, which is compared with the initial mass estimation of the aircraft. Note the masses of the BW structure are very close to each other with a maximum difference of about 15% for the vertical wing structures. This result is highly dependent on the type of connection between the three wing elements, which determine how the loads are transferred through the statically indeterminate structure. In this case, it was found that a fixed joint led to the lowest structural weight for the wing, which is consistent with previous analyzes of box-wing structures [43]. Overall, the Operational Empty Mass (OEM) increased about 2.35%, which increased the Fuel Mass (FM) for the nominal mission of about 2.68%. It is possible to conclude that the aircraft mass estimation introduced by Paerom provided appropriate results at conceptual design level.

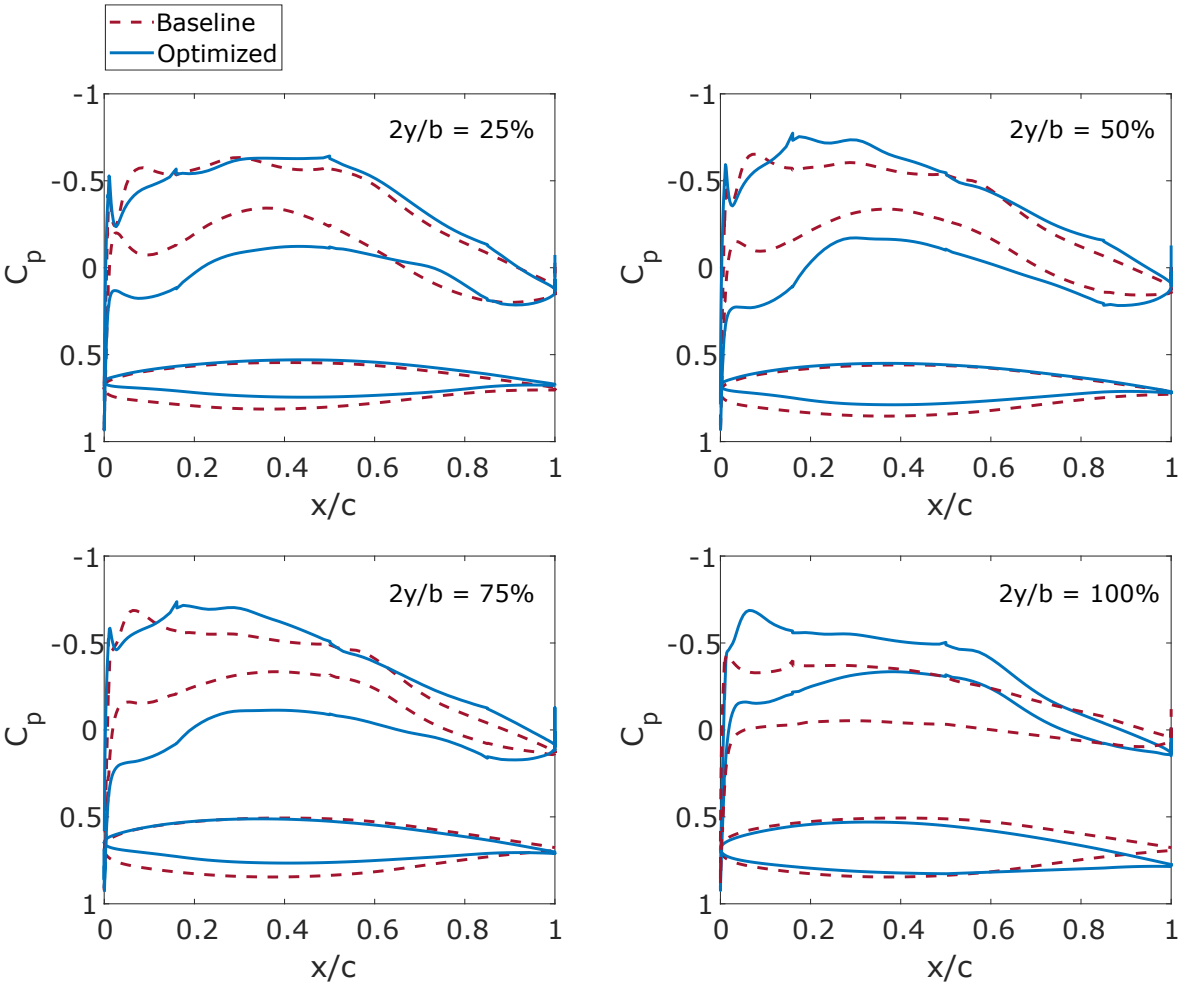

Figure 9 – Pressure distributions on the baseline and optimized box-wing designs (aft wing).

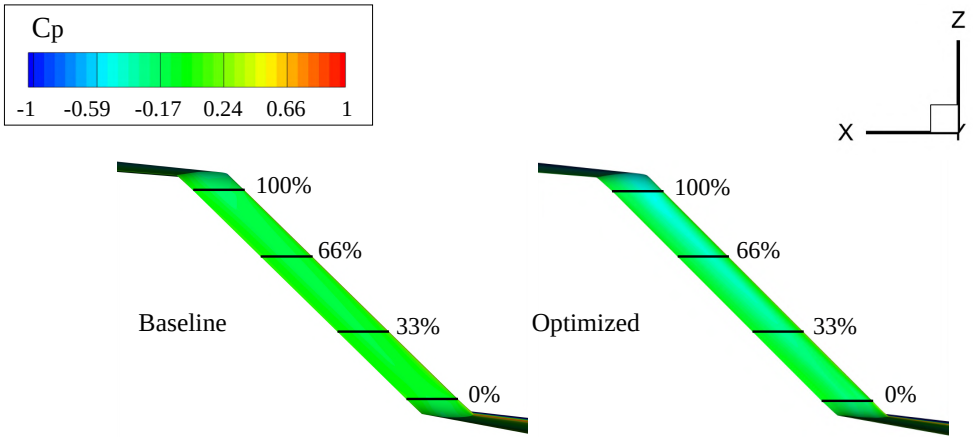

Figure 10 – Surface pressure coefficient contours for the baseline (left) and optimized (right) box-wing geometries (Lateral views of vertical wing).

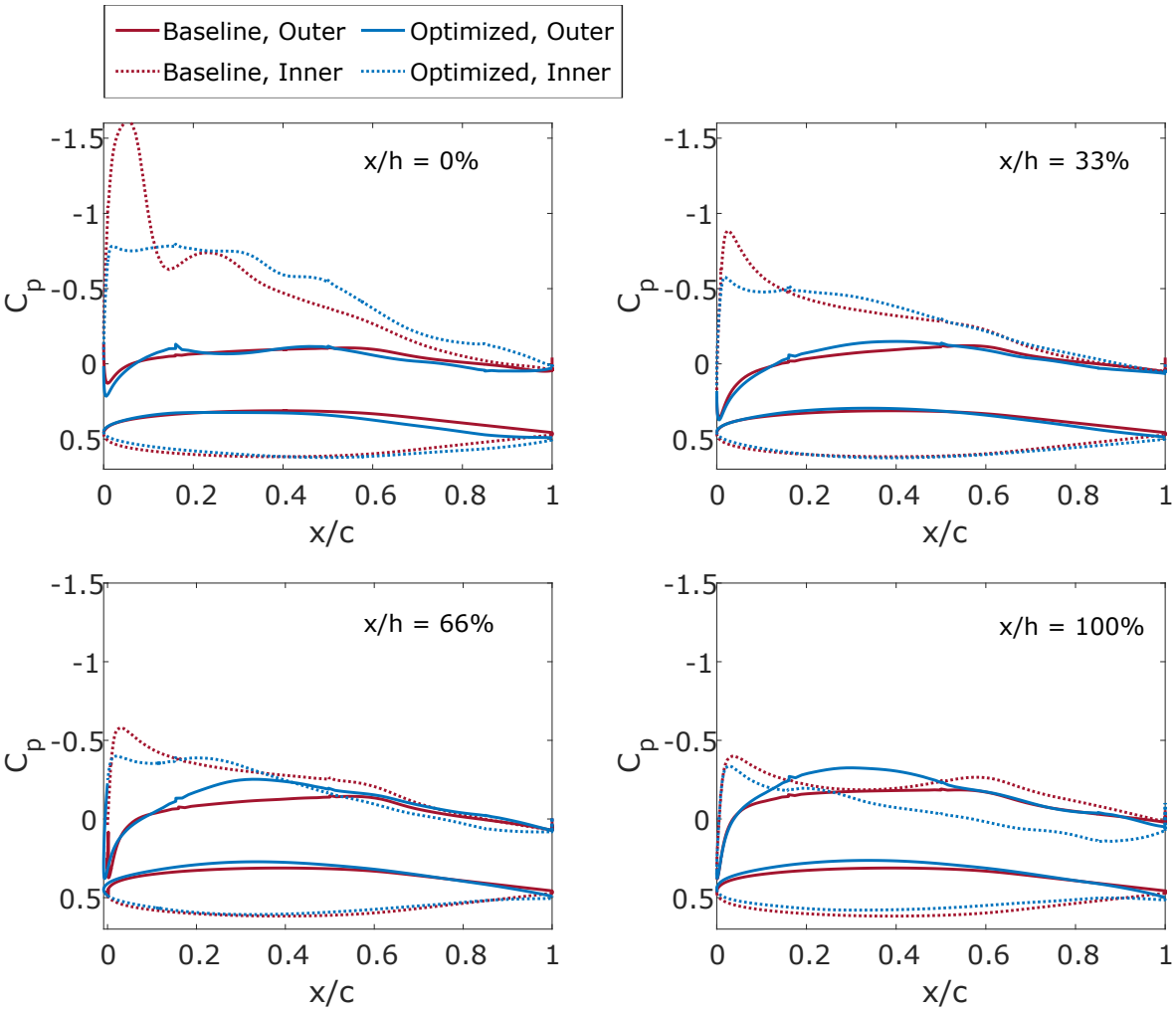

Figure 11 – Pressure distributions on the baseline and optimized box-wing designs (vertical wing).

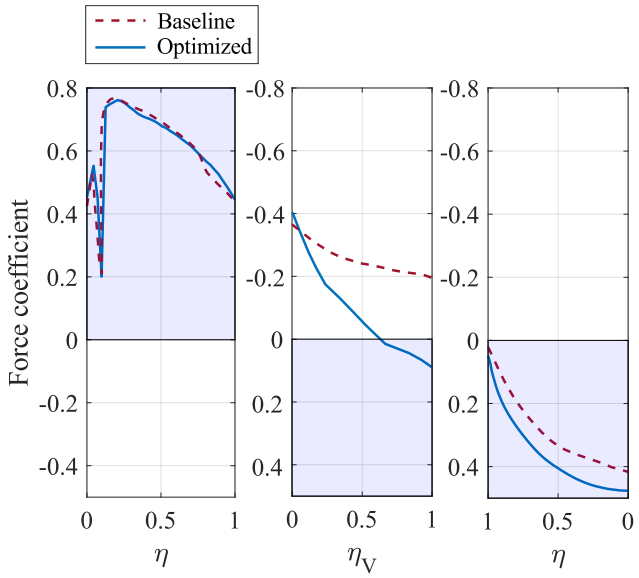

Figure 12 – Optimized force coefficient distributions over the fore wing (left), the vertical tip wing (middle), and the aft wing (right).

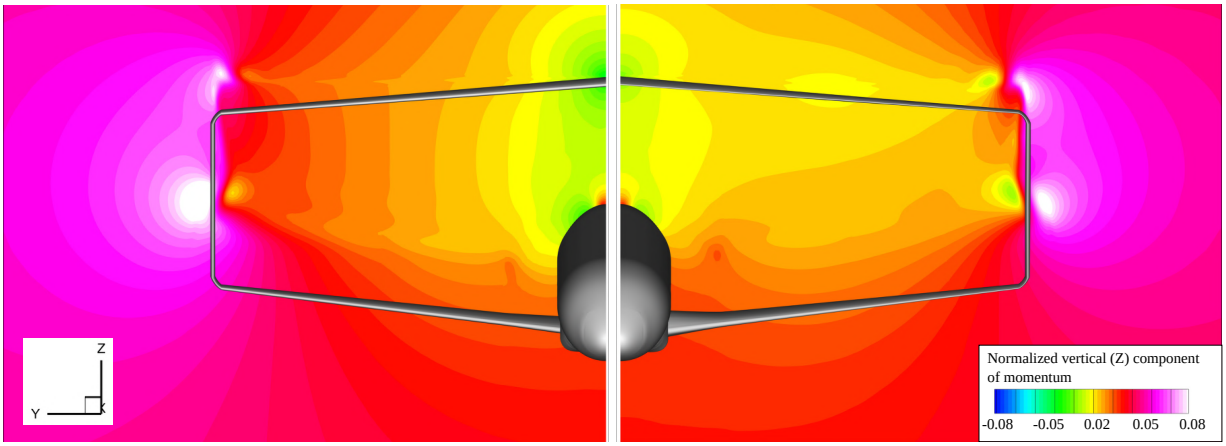

(a) Baseline. (b) Optimized.

Figure 13 – Plane cuts of the vertical component of momentum taken at 1 root-chord length downstream of the baseline and optimized box-wing configurations.

Table 5 – Mass breakdown of the BW concept in kilograms.

Parameter	**BW (Faber)**	**BW (Paerom)** [24]	Δ [%]
MTOW	80335.1	78978.8	+1.7
OEM	46067.2	44982.1	+2.3
Total Wing	10070.1	9990.4	+0.8
Fore wing	5204.8	5095.1	+2.1
Aft wing	4527.8	4495.6	+0.7
Tip fin	337.3	399.6	-15.5
Fuselage	8041.5	8247.8	-2.5
Vertical tail	752.1	746.0	+0.8
Landing gear	3155.5	3160.5	-0.1
Propulsion[1]	9002.1	8946.9	+0.7
Systems	11739.8	11646.9	+0.8
Operational items	2291.6	2273.4	+0.8
FM[2]	8104.2	7886.7	+2.7

[1] Includes bare engines, nacelles, and pylons.
[2] For nominal range plus diversion range (single-aisle category).

The flight simulation methods outlined by Bravo-Mosquera, Cerón-Muñoz, and Catalano [24] were used to evaluate the mission performance of the BW configuration in terms of fuel burn. A standard nominal mission for the single-aisle medium range category was analyzed, in which the aircraft transports 160 passengers and 5 crew over a distance of 1852 km at a Mach number of 0.78, with a 805 km fuel reserve. Fuel weights are mostly computed using the fuel fractions method. For takeoff (including warm-up and taxi), climb, and landing, the fuel fractions were taken from historical data. For cruise and loiter segments, the fuel fractions are given by the Breguet-range equation. Results from high-fidelity optimization plus a 5% markup on the skin friction drag component to account for excrescence drag from the vertical tail, nacelles, and pylons, are used to compute the Breguet-range equation for the specified mission profile.

The overall mission performance estimates are reported in Table 6. The optimized BW concept reduced drag by about 10% in comparison with the baseline BW, which reduced the fuel mass by about 5.3% for the specified mission profile. In contrast, a substantial drag reduction (about 14%) is obtained compared to the CTW aircraft.

5. Conclusions

This paper demonstrates the feasibility of high-fidelity aerodynamic shape optimization of a transonic box-wing aircraft using structured multiblock meshes and B-spline control points within free-form deformation volumes for geometry manipulation. This method was used to investigate the aerodynamic

Table 6 – Aircraft performance comparison.

Parameter	CTW[1,2]	BW[1] (Baseline)	BW[3] (Optimized)
L/D [-]	17.10	17.83	19.90
C_L [-]	0.59	0.51	0.51
C_D [-]	0.0344	0.0286	0.0256
Cruise Drag [N]	39634	38056	34064
Fuel Mass [kg]	8424	8287	7849

[1] Optimized using low-fidelity aerodynamics
[2] Aerodynamic data from CFD simulations.
[3] Optimized using high-fidelity aerodynamics.

design and fuel burn performance of a box-wing aircraft in the single-aisle medium-range category. In particular, a RANS-based aerodynamic shape optimization framework was applied to minimize cruise drag, with respect to angle of attack, twist, and section shape variables. Results show that a box-wing aircraft can be designed for low cruise drag, while satisfying both constant lift and zero pitching moment constraints through an optimum twist distribution and the elimination of shocks.

The optimized box-wing aircraft was found to provide a 10.4% improvement in cruise lift-to-drag ratio over the baseline concept, indicating that the features of the lifting system enable benefits in terms of reduction in fuel consumption per passenger. Such results demonstrate the feasibility of high-fidelity modeling to quantify the benefits of a box-wing aircraft and address several issues identified during the conceptual design stage.

6. Future work

- To fully assess the performance of the box-wing concept and provide meaningful insights, this proof-of-concept must be presented in a multiple operating point optimization level. By investigating the cruise operating point in isolation, the impact of the box-wing configuration at other operating points such as take-off, climb and landing are ignored. Therefore, it is important to allow for realising optimum designs with better capabilities at varying conditions.

- For the case considered here, optimal aerodynamic design features were found but with permissive considerations toward structural integrity. Maintaining minimum thickness-to-chord ratios across each wing may help in producing more feasible structural designs.

- Only the box-wing system and fuselage geometries were part of the current high-fidelity aerodynamic shape optimization application. This geometry aided to account for wing-body flow interactions and to correct for the less efficient lift provided by the fuselage. However, the vertical tail contribution must be considered in the design space, because this aerodynamic surface dictates the lateral-directional stability behavior, as well as the structural feasibility of this unconventional aircraft. A single vertical tail solution reduces the empty weight and wetted area, but it can be prone to potential aeroelastic problems. In contrast, a twin vertical tail solution increases the structural weight, and can be prone to shock formation and separation, but it represents a solution to aeroelastic instabilities.

- Finally, due to the unique characteristics of the box-wing concept, an aerostructural optimization process shall be investigated using parametric geometry modeling as a first step, providing control on the aircraft surfaces of this closed wing-system. An aerostructural design takes into account both aerodynamic and structural coupling, and therefore involves iterative and successive reevaluation of both the aerodynamic loads and structural design to come up with a coupled design. This methodology represents an interesting opportunity to the progress of the box-wing concept, since there are still unknowns about structural weight, flutter, and the specific nonlinear structural response that necessitates an unique buckling treatment.

7. Contact Author Email Address

mailto: pdbravom@usp.br

8. Copyright Statement

9. Acknowledgments

The authors disclosed receipt the following financial support for the research, authorship, and/or publication of this article: this work was financed by the National Council for Scientific and Technological Development - CNPq (grants 141950/2017-0 and 203402/2019-7).
Computations were performed on the Niagara supercomputer at the SciNet HPC Consortium. SciNet is funded by the Canada Foundation for Innovation under the auspices of Compute Canada; the Government of Ontario; the Ontario Research Fund - Research Excellence; and the University of Toronto.
The authors are grateful to Dr. Thomas Reist and Victor Alulema for their invaluable technical guidance and discussions on aerodynamic shape optimization using the Jetstream framework.

References

[1] Hileman, James I et al. “The carbon dioxide challenge facing aviation”. In: *Progress in Aerospace Sciences* 63 (2013), pp. 84–95.

[2] Bravo-Mosquera, Pedro D., Catalano, Fernando M., and Zingg, David W. “Unconventional aircraft for civil aviation: A review of concepts and design methodologies”. In: *Progress in Aerospace Sciences* 131 (2022), p. 100813. ISSN: 0376-0421.

[3] Park, Yongha and O’Kelly, Morton E. “Fuel burn rates of commercial passenger aircraft: variations by seat configuration and stage distance”. In: *Journal of Transport Geography* 41 (2014), pp. 137–147.

[4] Liebeck, Robert H. “Design of the blended wing body subsonic transport”. In: *Journal of aircraft* 41.1 (2004), pp. 10–25.

[5] Frediani, Aldo et al. “Conceptual design of PrandtlPlane civil transport aircraft”. In: *Proceedings of the Institution of Mechanical Engineers, Part G: Journal of Aerospace Engineering* (2019), p. 0954410019826435.

[6] Salem, Karim Abu et al. “A Physics-Based Multidisciplinary Approach for the Preliminary Design and Performance Analysis of a Medium Range Aircraft with Box-Wing Architecture”. In: *Aerospace* 8.10 (2021), p. 292.

[7] Tasca, Andrea et al. “Innovative Box-Wing Aircraft: Emissions and Climate Change”. In: *Sustainability* 13.6 (2021), p. 3282.

[8] Salem, Karim Abu et al. “Tools and methodologies for box-wing aircraft conceptual aerodynamic design and aeromechanic analysis”. In: *Mechanics & Industry* 22 (2021), p. 39.

[9] Carini, Marco et al. “Aerodynamic analysis and optimization of a boxwing architecture for commercial airplanes”. In: *AIAA Scitech 2020 Forum, AIAA 2020-1285*. Orlando, Florida, January 2020.

[10] Prandtl, Ludwig. “Induced drag of multiplanes”. In: *NATIONAL ADVISORY COMMITTEE FOR AERONAUTICS, Technical note NO. 182* (1924).

[11] Kroo, Ilan. “Nonplanar wing concepts for increased aircraft efficiency”. In: *VKI lecture series on innovative configurations and advanced concepts for future civil aircraft* (2005), pp. 6–10.

[12] Demasi, Luciano et al. “Minimum induced drag theorems for joined wings, closed systems, and generic biwings: Applications”. In: *Journal of Optimization Theory and Applications* 169.1 (2016), pp. 236–261.

[13] Russo, Lorenzo, Tognaccini, Renato, and Demasi, Luciano. “Box Wing and Induced Drag: Compressibility Effect in Subsonic and Transonic Regimes”. In: *AIAA Scitech 2020 Forum, AIAA 2020-0447*. Orlando, Florida, January 2020.

[14] Gagnon, Hugo and Zingg, David W. “Aerodynamic Optimization Trade Study of a Box-Wing Aircraft Configuration”. In: *Journal of Aircraft* 53.4 (2016), pp. 971–981.

[15] Gagnon, Hugo and Zingg, David W. “Euler-equation-based drag minimization of unconventional aircraft configurations”. In: *Journal of Aircraft* 53.5 (2016), pp. 1361–1371.

[16] Chau, Timothy and Zingg, David W. “Aerodynamic Shape Optimization of a Box-Wing Regional Aircraft Based on the Reynolds-Averaged Navier-Stokes Equations”. In: *35th AIAA Applied Aerodynamics Conference, AIAA 2017-3258*. Denver, Colorado, June 2017.

[17] Lange, RH et al. *Feasibility study of the transonic biplane concept for transport aircraft application*. Tech. rep. NASA-CR-132462. National Aeronautics and Space Admin Langley Research Center Hampton VA, 1974.

[18] Andrews, Stephen A and Perez, Ruben E. “Comparison of box-wing and conventional aircraft mission performance using multidisciplinary analysis and optimization”. In: *Aerospace Science and Technology* 79 (2018), pp. 336–351.

[19] Schiktanz, Daniel. “Conceptual design of a medium range box wing aircraft”. In: *Department Fahrzeug technik und Flugzeugbau, Master Thesis, Hamburg, HAW Hamburg* (2011).

[20] Jemitola, Paul Olugbeji. “Conceptual design and optimization methodology for box wing aircraft”. In: *Cranfield University, PhD Thesis, England* (2012).

[21] Garcia-Benitez, Jaime et al. “Conceptual design of a nonplanar wing airliner”. In: *Aircraft Engineering and Aerospace Technology: An International Journal* 88.4 (2016), pp. 561–571.

[22] Salam, Ishan Roy and Bil, Cees. “Multi-disciplinary analysis and optimisation methodology for conceptual design of a box-wing aircraft”. In: *The Aeronautical Journal* 120.1230 (2016), pp. 1315–1333.

[23] Bravo-Mosquera, Pedro D, Cerón-Muñoz, Hernan D, and Catalano, Fernando. “Design and computational analysis of a closed non-planar wing aircraft coupled to a boundary layer ingestion propulsion system”. In: *AIAA Propulsion and Energy 2019 Forum, AIAA 2019-3850*. Indianapolis, Indiana, August 2019.

[24] Bravo-Mosquera, Pedro D, Cerón-Muñoz, Hernán D, and Catalano, Fernando M. *Design, aerodynamic analysis and optimization of a next-generation commercial airliner*. Manuscript submitted for publication. 2022.

[25] Chau, Timothy and Zingg, David W. “Aerodynamic Design Optimization of a Transonic Strut-Braced-Wing Regional Aircraft”. In: *Journal of Aircraft* 59.1 (2022), pp. 253–271.

[26] Jemitola, PO, Monterzino, G, and Fielding, J. “Wing mass estimation algorithm for medium range box wing aircraft”. In: *The Aeronautical Journal* 117.1189 (2013), pp. 329–340.

[27] Hicken, Jason E and Zingg, David W. “Aerodynamic optimization algorithm with integrated geometry parameterization and mesh movement”. In: *AIAA Journal* 48.2 (2010), pp. 400–413.

[28] Gagnon, Hugo and Zingg, David W. “Two-level free-form and axial deformation for exploratory aerodynamic shape optimization”. In: *AIAA Journal* 53.7 (2015), pp. 2015–2026.

[29] Osusky, Lana et al. “Drag minimization based on the Navier–Stokes equations using a Newton–Krylov approach”. In: *AIAA Journal* 53.6 (2015), pp. 1555–1577.

[30] Pironneau, Olivier. “On optimum design in fluid mechanics”. In: *Journal of fluid mechanics* 64.1 (1974), pp. 97–110.

[31] Jameson, Antony. “Aerodynamic design via control theory”. In: *Journal of scientific computing* 3.3 (1988), pp. 233–260.

[32] Gill, Philip E, Murray, Walter, and Saunders, Michael A. “SNOPT: An SQP algorithm for large-scale constrained optimization”. In: *SIAM review* 47.1 (2005), pp. 99–131.

[33] Reist, Thomas A and Zingg, David W. “High-fidelity aerodynamic shape optimization of a lifting-fuselage concept for regional aircraft”. In: *Journal of Aircraft* 54.3 (2016), pp. 1085–1097.

[34] Reist, Thomas A et al. “Multifidelity Optimization of Hybrid Wing–Body Aircraft with Stability and Control Requirements”. In: *Journal of Aircraft* 56.2 (2019), pp. 442–456.

[35] Hicken, Jason E and Zingg, David W. “Parallel Newton-Krylov solver for the Euler equations discretized using simultaneous approximation terms”. In: *AIAA Journal* 46.11 (2008), pp. 2773–2786.

[36] Fernández, David C Del Rey, Hicken, Jason E, and Zingg, David W. “Review of summation-by-parts operators with simultaneous approximation terms for the numerical solution of partial differential equations”. In: *Computers & Fluids* 95 (2014), pp. 171–196.

[37] Spalart, Philippe and Allmaras, Steven. “A one-equation turbulence model for aerodynamic flows”. In: *30th aerospace sciences meeting and exhibit*. 1992, p. 439.

[38] Osusky, Michal, Boom, Pieter D, and Zingg, David W. “Results from the Fifth AIAA Drag Prediction Workshop obtained with a parallel Newton-Krylov-Schur flow solver discretized using summation-by-parts operators”. In: *31st AIAA Applied Aerodynamics Conference, AIAA 2013-2511*. San Diego, California, June 2013.

[39] Kenway, Gaetan KW et al. “Effective adjoint approaches for computational fluid dynamics”. In: *Progress in Aerospace Sciences* (2019), p. 100542.

[40] Finlayson, M A. “ANSYS ICEM CFD User’s Manual”. In: *ANSYS, Inc. Canonsburg, PA, Nov*. 2013.

[41] Demasi, Luciano, Monegato, Giovanni, and Cavallaro, Rauno. “Minimum induced drag theorems for multiwing systems”. In: *AIAA Journal* 55.10 (2017), pp. 3266–3287.

[42] Torenbeek, Egbert. *Advanced aircraft design: conceptual design, analysis and optimization of subsonic civil airplanes*. John Wiley & Sons, 2013.

[43] Jemitola, PO, Fielding, J, and Stocking, P. “Joint fixity effect on structural design of a box wing aircraft”. In: *The Aeronautical Journal* 116.1178 (2012), pp. 363–372.